Comparison of Multidimensional Hyperspectral Image with SIFT Image Mosaic Methods for Mosaic Better Accuracy

G. Suseendran, E. Chandrasekaran, Souvik Pal, V. R. Elangovan, and T. Nagarathinam

Abstract Hyperspectral images can offer a lot of clarity by blending both spectral and spatial data. Details are for the researcher. A multidimensional paper in this paper, the hyperspectral image mosaic solution, was suggested to properly assemble hyperspectral images. This approach is a synthesis of texture details of the single gray picture, the hyperspectral spatial details image, and location details obtained during the purchase phase. This method is used in the world of medicine. Image and experimental findings hyperspectral suggest that this technique is useful compared to other image mosaic approaches based on the line segment function of scale-invariant feature transform (SIFT).

Keywords Hyperspectral imaging · SIFT

G. Suseendran (✉)
Department of Information Technology, Jeppiaar Engineering College, Chennai, India

E. Chandrasekaran
Department of Mathematics, Vel Tech Rangarajan Dr. Sagunthala R&D Institute of Science and Technology, Chennai, India

S. Pal
Department of Computer Science and Engineering, Global Institute of Management and Technology, Krishnanagar, India

V. R. Elangovan
Department of Computer Applications, Agurchand Manmull Jain College, Meenambakkam, Chennai, India

T. Nagarathinam
PG and Research Department of Computer Science, MASS College of Arts and Science, Kumbakonam, India

© The Author(s), under exclusive license to Springer Nature Singapore Pte Ltd. 2021

S.-L. Peng et al. (eds.), *Intelligent Computing and Innovation on Data Science*,
Lecture Notes in Networks and Systems 248,
https://doi.org/10.1007/978-981-16-3153-5_23

1 Introduction

Classification of hyperspectral images solves the issue of identifying land-cover groups and thematic production of maps with broad applications in precision agriculture, mining discovery, environmental monitoring, etc. It usually consists of several main phases, sampling, preprocessing of data, extraction of features, and model building. Among those measures, extraction of features is of great importance, and goals are to find the most lightweight and detailed set of functions to boost the classification tasks' accuracy and reliability. The thematic map also suffers from salt and pepper noise due to noise in hyperspectral data [1]. The two-dimensional photographs can be applied to spectral as a further dimension of information. In the sector, the resulting spectral imager was commonly used for monitoring climate and modern agriculture [2]. The categorization of hyperspectral images was formulated from the point of view of segmentation and classification tasks [3].

Spectral image feature classification is an active field of visual image analysis study. The feature is due to the dataset's high dimensionality. Classification is a low-precision and complex task—the use of traditional methods. A variety of research projects have shown their participation. Spatial details in the extraction process of features may be required to increase the description of hyperspectral image accuracy [4] significantly. Details on the three-dimensional image has only points on the morphological structure. It has only points on the morphological structure. At the same time, the hyperspectral image has details on tissue components. It is commonly used in the field of remote sensing and also in the medical area fields. Some used a hyperspectral representation of the pig's blood vessel to make a successful differentiation between arteries and veins classification approach for the support vector machine [5].

(SIFT) David G. Lowe suggested that it has been proven to be the most durable among the other descriptors of local invariant features concerning various geometrical changes. What are the functions invariant for rebalancing, localization and respective user, and partly invariant lighting shifts and Affine or 3D visualization. For a particular benefit, SIFT functionality can be used in image-matching applications Performed in many areas, such as anti-spam [6]. SIFT is an algorithm that translates image data to local the function of the vector. These features have geometric robustness transformations such as localization, scaling, and rotation [7].

To achieve this, we suggested a hybrid process. Take advantage of the two approaches described above, scale-invariant function transform (SIFT) and multdimensional hyperspectral image for mosaic method. This approach synthetically uses texture knowledge, hyperspectral information, and location information obtained at the technique, and when comparing the two above methods, we can get which one produces better results.

2 Related Works

Zhu and Ren [8] suggested a modern picture mosaic technology based on the scale-invariant aspect transform (SIFT) line segment feature to overcome event scaling, rotation, lighting state changes, etc, the technique of mosaics. The Harris corner detector operator uses this method first to detect key points. Secondly, it creates directed line segments, recognizes them with the SIFT function, and meets those guided segments in the rough-point matching acquisition.

Datta and Chakravorty [9]—The goal of hyperspectral image segmentation is to minimize the challenge of evaluating hyperspectral data by dividing the image into categories dependent on correlations within homogenous or spectral areas. The segmentation method is one of the first steps in the distance sensing analysis of the image; the image is separated into regions that reflect the objects in the image better.

Hu and Ai [10]—SIFT based on image attribute extraction and primary point matching approach is suggested. A wide-angle spinning triangle shift images are measured from unmanned aerial vehicles (UAV). It has a far wider use than conventional aerial photogrammetry as a particular low-altitude UAV photography process based on the concept of photogrammetry.

Mendlovic and Raz [11] said that common imaging systems based on silicone benefit in-depth and spectral data by significant resolution penalties. However, compact detection methods eliminate the liability for computer cameras and involve upgraded optical equipment and preliminary information reliance. This paper lays forth a new idea for a positive imaging system: color and hyperspectral imagery multiplex and compressed images.

3 Methodology

3.1 Multidimensional Hyperspectral

In Fig. 1, the workflow for our algorithm is shown. First of all, for each hyperspectral band, we pick the comparison band as one band. Imagine and calculate the processing matrix of the two hyper-speed images. Depending on the phase, Up the Robust Attribute (SURF) function reference band then the pair. Depending on the auxiliary bands and their change, the bands are selected. The matrix is calculated in the same manner and stored for further predictions [12]. We use additional location information to filter off matrices to delete the second level's error matrix. To use this fusion matrix, we calculate the merger filtered matrix in the fourth step. Stitch the images hyperspectrally.

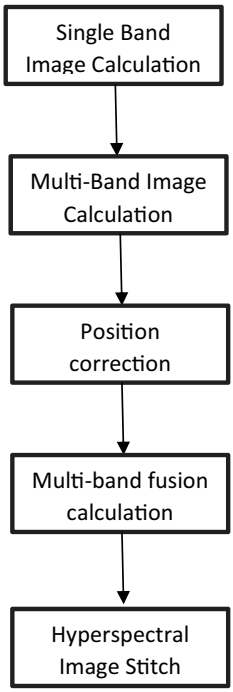

Fig. 1 Workflow of algorithm

3.1.1 Definition of the Framework

The following method, seen in Fig. 2, captures the hyperspectral image that we used in this article.

This sample machine hyperspectral picture is referred to below and above. Electronic dot, AOTF, gray science CMOS(sCMOS) camera, color charging coupled device (CCD), light splitter, and modern computing devices are the traditional optical microscope methods. Typical optical microscope systems [13].

The image of the slide is visible immediately in the optical microscope, like all microscopes. Also, it can be relocated to capture devices like SCMOS and CCD. This is the light splitter that is used to pick a picture system through a button. The stage can be controlled by hand, or power orders can be accessed from industrial computers. Oh, machine. Oh, machine. The acoustic-optical tunable filter will filter the target light frequency using a self-adjustment. The computer obtains computer and electronic level conditions sCMOS/CCD image.

3.1.2 Registration Picture

Image registration is one of the most effective procedures in the mosaic of images. By recognition and matching features, many images have been transformed into the

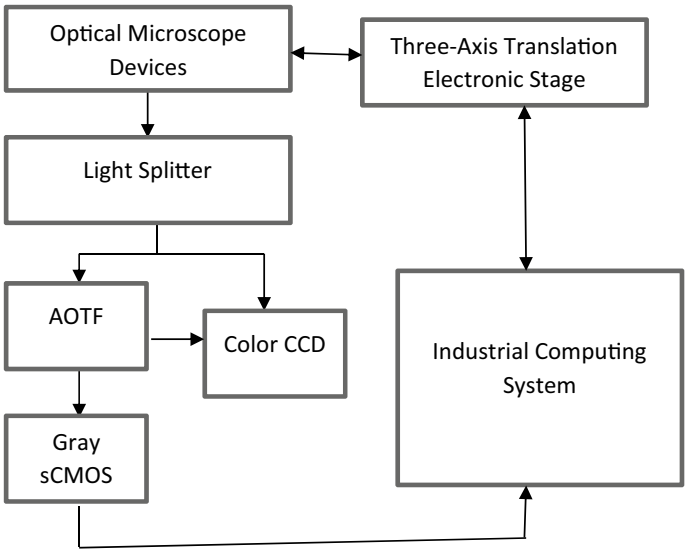

Fig. 2 Hyperspectral image sample system

same coordinate system. You may define the algorithms used as field-based and practical methods in this method. The feature-based solution has been proposed in the past few years by various people [14]. Thanks to the opportunity to handle the transition of a few pictures' scales and rotation for ten years and perform a far more critical role in the picture registry than field-based approaches.

3.1.3 Selection of the Reference Image

For both of us, we pick each picture hyperspectral pictures {H1, H2} on the band Bref as the reference image(Iref) that is valid, which is seen in Fig. 3. We are denoting that these two pictures are in H1, H2as IBref1, IBref2. In practice Bref no, the following formula is derived:

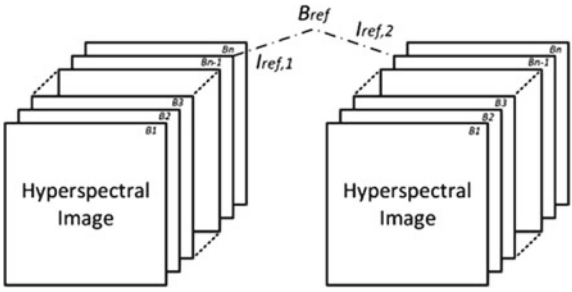

Fig. 3 Hyperspectral image illustration

$$B_{\text{ref}} = (B_{\text{start}} + B_{\text{end}})/2 \quad (1)$$

3.1.4 Function Identification and Connection

In this document, we are applying the SURF function-based approach for estimating the matrix of two hyperspectral pictures. Function points for two photographs SURF, which is resilient against the SURF, are detected by IBref1 and IBref2, scaling and rotation. Each function point includes 64 descriptors carrying knowledge about the surrounding environment, so that it is possible to, as a vector, see any point. Each picture has dimensions of NBref*64, and the Iref number is NBref. Concerning K, the characteristics show the nearest relative. Algorithm to find a relationship between two features of the matrix {ABref1, ABref2}. There will be some points during this process unmatched owing to the image's self-correlation [15].

RANSAC is used to solve this discrepancy condition and to achieve a robust estimate of the MBref transition matrix. MBref is the matrix of transformation between IBref1 and IBref2.

3.1.5 Matrix Fusion Transform

Calculations for multi-band: Relevant spectrum descriptions are given by each pixel in the hyperspectral system imaging—for frames properties of a hyperspectral image and the object under either wavelength illumination. This adds to the circumstance in which each image has information different from other artists, with its contrast and texture. Therefore, only one pair of gray images active in the computation process can lead to the mosaic's uncertain result [16].

Correction of place: Poor contrast or lack of texture information on specific pictures can turn out to be non-normal. Transformation matrixes interact with the final fusion process matrix, guy [17]. We are importing additional location information to sort these non-normal matrices. Place details shall be gathered throughout. The method of image capture contains a three-axis coordinate details for each graphic. The course of scanning hyperspectral representations is shown in Fig. 4.

Only one path may contain two adjacent images. As seen in Fig. 4, change the x- or y-axis. For the matrix to be corrected, only the x and y coordinates are used, while the z-axis is used to correct the matrix. The focal length of this phase we do not care about. There are also two x-y offsets used in the transformation matrix. Photographs are parallel. We map the physical distance between the two of us by using the following formula to point to the distance of the pixel in the image:

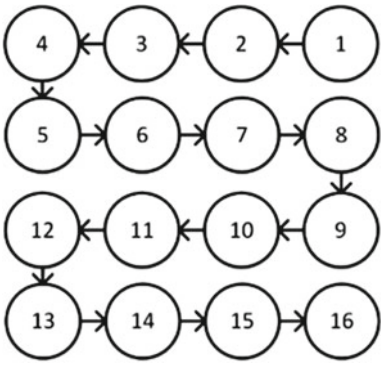

Fig. 4 Direction of scanning

$$a = \frac{L_{\text{pixel}}}{L_{\text{physical}}} \tag{2}$$

L_{pixel} it can be determined as follows:

1. Single image capture, three-axis electronic phase transition via L_{physical} value. The value of another picture is being arrayed and filmed.
2. For two images, calculate the transformation matrix.
3. In the matrix, the x/y offset value is L_{pixel}.

Algorithm 1. For finding Mpos

1. Input; dxBl1,dyBl1. Assume the (dxBl1,dyBl1) as the x-y offset in the transformation matrix MBl1.
2. If dyBl1 = 0
3. Then a* L_{physical} * 0.9 * < dxBl1 < a* L_{physical} * 1.1
4. If dxBl1 = 0
5. Then a* L_{physical} * 0.9 * < dyBl1 < a* L_{physical} * 1.1
6. Find Mpos
7. $$\text{Mpos} = \sum_{i=1}^{m} \beta_i * M_{\text{Bli}} \tag{3}$$

and

$$\sum_{i=1}^{m} \beta_i = 1 \tag{4}$$

8. If m = n,
9. Then $\beta_i = \beta_{\text{init}}$
10. If m $\neq$ n
11. Then $\beta_i = \beta_{\text{init}} + \beta_{\text{step}} * (i = 1), 1 \leq i \leq u$
12. Result Mpos is calculated as {MBl1, MBl2,…MBlm}

The fusion matrix. A relative error to produce a fusion matrix which specifies between M_{pso}, M_{ref} is as follows:

$$M_{\text{err}} = \left(M_{\text{pos}} - M_{\text{ref}}\right)/M_{\text{ref}} \tag{5}$$

$$M_{\text{fusion}} = x * M_{\text{ref}} + (1 - x) * M_{\text{pos}} \tag{6}$$

where x = 1/2, if o <=err < 0.1

x = 1-err*2, if 0.1 <=err < 0.5

x = 1,err =>0.5

To obtain the merger for the image pairs, we use Eq. 6, and we will get {IBl1,1, IBl1,2}, {IBl2,1, IBl2,2}, and {IBln,1, IBln,2}.

Figure 5 shows the multidimensional hyperspectral images for the mosaic method of the input images.

Figure 6 shows the resulted images we got and we deliver in pairs with the original input images to show the accuracy, as given in Table 1 and Fig. 7.

3.2 SIFT

Image pyramid building, in-depth recognition of key points and others which take a lot of time since the SIFT technique is used to detect characteristic points. The Harris operator's benefits are to locate the corner points and speed up the mosaic recognition with the Harris method with the combination of the feature points with the SIFT picture definition.

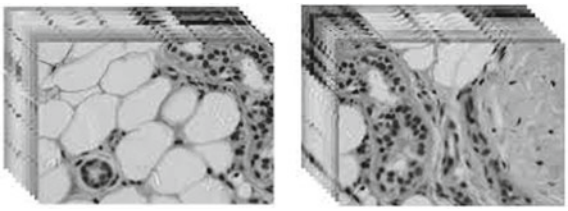

Fig. 5 Hyperspectral images for the experiment

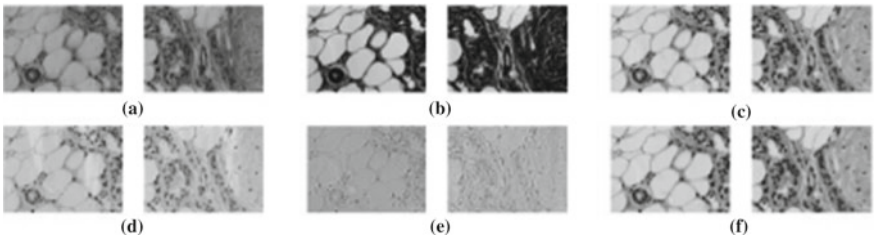

Fig. 6 Pair images we got after the result

Table 1 Accuracy for the multidimensional hyperspectral images

Images	Input image	Output image
a	33.4	90.5
b	44.1	94.7
c	36.5	91.6
d	45.7	96.1
e	56.3	97.2
f	49.4	91.2

Fig. 7 Graph for the multidimensional hyperspectral images

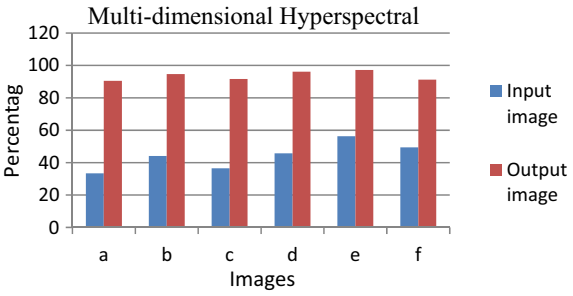

3.2.1 Detection of Harris Corner

The Harris customer is a Chris Harris type proposed by a signal-based point removal operator with simple estimates, extraordinarily generous and rational angles, probable quantitative extraction, and a reliable operator. Its detection method for the Harris Corner uses the feature of the signal processing theory, which describes both the peak in the high line and high line curvature [1] Phase Harris can be seen as:

$$M = G(s\sim) * \begin{bmatrix} g_x^2 & g_x g_y \\ g_x g_y & g_y^2 \end{bmatrix} \tag{7}$$

Of which g_x means the gradient direction at x, g_y means the gradient direction at x. $G(s)$ at Gaussian means Gaussian prototype at y-direction gradient, (*) implies the stress between the Gaussian template and function.

3.2.2 Point Matching

We achieve the matching of the line segments by the law of the closest neighborhood. More point accuracy is required to match the accurate image mosaic. We use a method based on mathematical voting in two images, $V = \{a1, a2, \ldots, an\}$ and $V = \{b1, b2, \ldots bm\}$, Key Kit Points. For frequency of point matching to be reached. If we note, if there are two, their starting point and their stopping point, the straight lines match each other. The argument is supposed to be matched. Initiate a first-place null matrix statistical matrix G to Rnm; the G form is defined in procedure 2. In the G matrix, the higher factor value suggests a higher likelihood of the matching point. The criteria for choosing the corresponding points are:

Algorithm 2. Computation procedure of matrix K.

1. Initialize $K \in Rn1 \times n2$ into null matrix
2. For $i = 1, 2, \ldots, n1$ If $lj1$ is k neighboring point of li, $K(i, j) = 1$
3. Output k

Algorithm 3. Computation procedure of matrix G.

1. Initialize $G \in Rn \times m$ into null matrix
2. For $i = 1, 2, \ldots, n1$, $j = 1, 2, \ldots, n2$
   (i) If $K(i, j) = 1$
   (ii) According to the directed line segment li is $al \rightarrow am$, the directed line segment $l\,j$ is $bp \rightarrow bq$
   (iii) $G(l, p) = G(l, p) + 1$, $G(m, q) = G(m, q) + 1$
3. Output matrix G

1. $G(i,j) > 5\text{-}007$, of which 5-007 corresponds to the proper positive number;
2. pick the point for each column corresponding to the principal elements of each row. Step, $G(i,j) >$ ala, in which ala is a successful pass. Number if the elements in row I and J are the same, as in $G(i,j)$. The number is the same for all elements in row I and ;

(3) If there is a Factor limit in row, I and the element cap are not the same in column j. Choose one randomly; choose a limit, for example. For each Othering, elements in rows I $G(i, q)$, ai, and bq fit; sets all elements in row I and column q to be zero,

Table 2 Accuracy of multidimensional hyperspectral images and SIFT

Images	Hyperspectral	SIFT
a	90.5	88.2
b	94.7	90.2
c	91.6	87.3
d	96.1	91.5
e	97.2	92.3
f	91.2	86.4

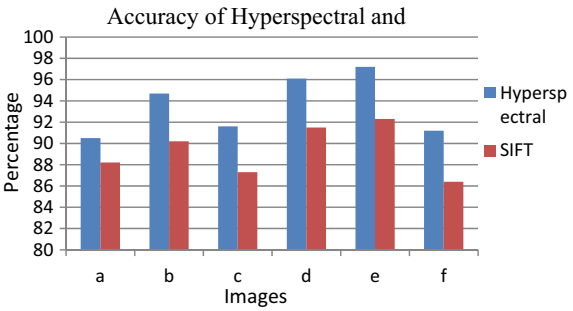

Fig. 8 Accuracy of multidimensional hyperspectral images and SIFT

From Table 2 and Fig. 8, we can conclude that the accuracy of the input images that we experimented on multidimensional hyperspectral images and SIFT for mosaic method shows that the multidimensional hyperspectral accuracy images are more significant than the SIFT mosaic method.

4 Conclusion

This paper proposes enhancing the precision of the mosaic image in a solid multidimensional mosaic image solution. The issue of misalignment in the photographic field is eliminated by photography and additional details on the positioning. Redundancy of hyperspectral spatial data is the experiment presentations showing that the suggested solution is successful in multiple image mosaic problems. This technique can also be found in certain spatial information redundancy implementations for image mosaics for some of you. We experimented on multidimensional hyperspectral images, and SIFT for mosaic method shows that the accuracy of the multidimensional hyperspectral images is greater than the SIFT mosaic method.

References

1. Liang J, Zhou J, Gao Y (2016, September) Tensor morphological profile for hyperspectral image classification. In: 2016 IEEE international conference on image processing (ICIP), pp 2197–2201. IEEE
2. Luo J, Cai F, Yao X, Li J, Huang Q, He S (2020) Experimental demonstration of an anti-shake hyperspectral imager of high spatial resolution and low cost. *IEEE* Sens J
3. Priego B, Duroy R (2018, September) Amigo: a tool for the generation of synthetic hyperspectral images. In: 2018 9th workshop on hyperspectral image and signal processing: evolution in remote sensing (WHISPERS), pp 1–5. IEEE
4. Wang Y, Cui S (2014, July) Hyperspectral image feature classification using stationary wavelet transform. In: 2014 international conference on wavelet analysis and pattern recognition, pp 104–108. IEEE
5. Huang Y, Zhou M, Li Q, Liu H, Guo F (2016, October) A multi-dimensional microscopic imaging system and reconstruction methods. In: 2016 9th international congress on image and signal processing, biomedical engineering and informatics (CISP-BMEI), pp 576–580. IEEE
6. Chen J, Zhang L, Lu Y (2008, December) Application of scale invariant feature transform to image spam filter. In: 2008 second international conference on future generation communication and networking symposia, vol 3, pp 55–58. IEEE
7. Baykal E, Ustubioglu B, Ulutas G (2016, June) Image forgery detection based on SIFT and k-means++. In: 2016 39th international conference on telecommunications and signal processing (TSP), pp 474–477. IEEE
8. Zhu J, Ren M (2014) Image mosaic method based on SIFT features of line segment. Comput Math Methods Med
9. Datta A, Chakravorty A (2018, October) Hyperspectral image segmentation using multi-dimensional histogram over principal component images. In: 2018 international conference on advances in computing, communication control and networking (ICACCCN), pp 857–862. IEEE
10. Hu Q, Ai M (2011, June) A scale invariant feature transform based matching approach to unmanned aerial vehicles image geo-reference with large rotation angle. In: Proceedings 2011 IEEE international conference on spatial data mining and geographical knowledge services, pp 393–396. IEEE
11. Mendlovic D, Raz A (2015, August) Multi-dimensional hyperspectral imaging system. In: *2015* International conference on optical MEMS and nanophotonics (OMN), pp 1–2. IEEE
12. Cheung W, Hamarneh G (2007, April) N-sift: N-dimensional scale invariant feature transform for matching medical images. In: 2007 4th IEEE international symposium on biomedical imaging: from nano to macro, pp 720–723. IEEE
13. Bedruz RA, Sybingco E, Quiros AR, Uy AC, Vicerra RR, Dadios E (2016, November) Fuzzy logic based vehicular plate character recognition system using image segmentation and scale-invariant feature transform. In: 2016 IEEE region 10 conference (TENCON), pp 676–681. IEEE
14. Chen Q, Kotani K, Lee F, Ohmi T (2008, December) Scale-invariant feature extraction by VQ-based local image descriptor. In: 2008 international conference on computational intelligence for modelling control & automation, pp 1217–1222. IEEE
15. Setiawan W, Wahyudin A, Widianto GR (2017, October) The use of scale invariant feature transform (SIFT) algorithms to identification garbage images based on product label. In: 2017 3rd international conference on science in information technology (ICSITech), pp 336–341. IEEE
16. Pal S, Bhattacharyya S, Doss S, Akila D, Suseendran G (2019) Hyperspectral and multispectral image fusion using NSCT and FDCT methods. J Crit Rev 7(5):2020
17. Qinglong H, Zhang Y, Hongbo L, Tianjiao F (2017, May) A novel target tracking method based on scale-invariant feature transform in imagery. In: 2017 international workshop on remote sensing with intelligent processing (RSIP), pp 1–5. IEEE